Observation of Cross-Field Transport of Pellet Plasmoid in LHD

Ryuichi SAKAMOTO and Hiroshi YAMADA
National Institute for Fusion Science, Toki, Gifu 509-5292, Japan
(Received 8 March 2011 / Accepted 29 May 2011)

A three-dimensional observation of the solid hydrogen pellet ablation has been performed by using a fast stereo imaging camera to investigate the pellet ablation dynamics. The initial velocity component of the injected pellet is maintained during ablation in a hot plasma, and the pellet penetrates to the core plasma. On the other hand, it has been observed that part of high density pellet plasmoid, which is formed around the pellet substance by ablating hydrogen pellet, intermittently breaks away from the pellet ablating position and the breakaway plasmoid is transported across a confinement field. The breakaway plasmoid recurrently develops at the rate of about 100 times per millisecond and it is non-diffusively transported approximately 0.1 m during its several 10 μs lifetime in the opposite direction to the pellet motion, namely, toward the low magnetic field side. This observation gives a reasonable explanation for the difference between the pellet ablation position and the effective particle deposition profile.

Keywords: pellet, fueling, ablation, plasmoid, non-diffusive transport

DOI: 10.1585/pfr.6.1402085

1. Introduction

Solid hydrogen pellet injection can directly provide fuel particles to a high temperature plasma, and therefore it is one of the promising candidates for fueling a fusion reactor. Decades of continuous efforts have been made from both theoretical and experimental aspects in the field of the pellet injection fueling [1, 2]. Nevertheless, there is room for further investigation into core fueling under fusion reactor conditions. The main difficulties are the shortening of the pellet penetration length as plasma temperature increase and the rapid transport of pellet ablatant toward the low magnetic field direction. The former can be solved through larger-mass and/or higher-speed pellet injection. However, since applicable pellet mass is restricted by acceptable density increment of the target plasma, the pellet mass cannot be determined arbitrarily. In regard to the pellet velocity, although it can be determined arbitrarily, the pellet penetration length scaling shows that the higher speed injection is less effective [3] and there are technological difficulties to increase the pellet velocity. The latter can be utilized to advantage by optimizing the pellet injection location and it has been confirmed in tokamaks that the high field side pellet injection can improve effective pellet fueling performance [4, 5]. The $\nabla \boldsymbol{B}$ induced drift model is widely accepted as the mechanism of the pellet plasmoid drift toward the low magnetic field direction in tokamak devices [6–8], and the ITER plasma fueling system relies on the high field side pellet injection [9].

As mentioned above, an effective fueling property depends not only on how far a pellet can penetrate into the hot plasma but also on how ablated particles are transported during the homogenization process into the background plasma. In order to extrapolate a fueling scenario into a future fusion reactor, therefore, it is important to understand the dynamics of a high density plasmoid which is composed of pellet ablated material. The initial stage of the plasmoid movement has been observed using a two-dimensional framing camera in TEXT [10], while the author did not refer to the possibility of $\nabla \boldsymbol{B}$ induced drift because there had been no such notion at that time. The dynamics of the plasmoid have been observed directly by use of a one-dimensional fiber optics array in RTP and ASDEX-upgrade [11, 12], and the rapid transport of the pellet plasmoid toward magnetically low field side has been confirmed. So far the observation of the plasmoid has been conducted by using a one- and/or two-dimensional field of view as mentioned above. What seems to be lacking, however, is spatial localization along the line of sight. Although one-dimensional observation is reasonable if the major radially outward drift which is predicted by theoretical models is secured, the direction does not necessarily correspond to the major radius if there are some non-ideal effects which are not considered in the models. In order to make a detailed study of the plasmoid dynamics, therefore, three-dimensional observation is one of the useful measures. In particular, a stellarator which has a three-dimensional magnetic field structure requires three-dimensional observation because the direction of $\nabla \boldsymbol{B}$ varies from one locality to another and the direction of the plasmoid transport must change depending on its position.

This paper presents the initial results of a three-dimensional observation of the solid hydrogen pellet ablatant by applying a stereoscopic method to fast camera

author's e-mail: sakamoto@LHD.nifs.ac.jp

observation on the Large Helical Device (LHD).

2. Experiment Set-up

Pellet injection experiments have been performed in LHD, which is a heliotron-type fully superconducting device with a pair of $\ell/m = 2/10$ continuous winding helical coils and three pairs of poloidal coils. Representative major radius, averaged plasma minor radius and magnetic field strength are 3.9 m, 0.6 m and ≤ 3 T, respectively. Since the entire confining magnetic field is generated by external coils, a considerable helical ripple with a three-dimensional effect dominates the confinement field in addition to an axisymmetric toroidal field. Since the helical coils dominate the confining magnetic field, the magnetically high field side is located around the coils and therefore the inboard side is not necessarily the high field side. In this study, the pellet is injected from the outboard side in the horizontally elongated poloidal cross section as shown in Fig. 1, and this injection location is the low field side from the viewpoints of both the toroidal and helical ripple effects. Typical pellet size and velocity are 2.7 mmϕ (0.6×10^{21} atoms) and 500 m/s, respectively.

The target plasmas were NBI (Neutral Beam Injection) heated plasmas with total a port-through power of $P_{\mathrm{NBI}} = 12$ MW. Three NBIs are tangentially injected with a beam energy of $E_{\mathrm{NBI}} = 180$ keV. Target plasma temperature and density are $T_e(0) = 2$ keV and $\bar{n}_e = 2 \times 10^{19}$ m^{-3}, respectively.

A fast imaging camera and a bifurcated imaging optical fiberscope are employed for the stereo observation as shown in Fig. 1. The two object lenses on the bifurcated ends of the imaging optical fiberscope are mounted viewing in the direction of the pellet trajectory with a separation of 1.24 m. The axis which originates at the mid point between the two observation points is defined as the Z axis. The direction of the pellet injection coincides with the Z axis and is opposite to the direction of the major radius, namely, $R = 7.1 - Z$. A pair of stereo images, which are taken by the bifurcated imaging optical fiberscope, has been focused onto the single fast imaging camera's focal plane, to ensure the simultaneity of both images. Dynamic range, spatial resolution, frame rate and exposure time of the fast camera are 12 bit, 464 × 192 pixels, 20,000 fps (frame per second) and 2 - 10 μs, respectively. Since the projection matrices of the fast camera observation system, i.e. $\boldsymbol{P}_{\mathrm{L}}$ and $\boldsymbol{P}_{\mathrm{R}}$ were calibrated previously [13], a three-dimensional spatial point $\boldsymbol{M} = [X\,Y\,Z]^T$ can be estimated from a pair of corresponding two-dimensional image points $\boldsymbol{m}_{\mathrm{L}} = [u_{\mathrm{L}}\,v_{\mathrm{L}}]^T$ and $\boldsymbol{m}_{\mathrm{R}} = [u_{\mathrm{R}}\,v_{\mathrm{R}}]^T$ on the both images by solving the following simultaneous equations.

$$\begin{cases} \tilde{\boldsymbol{m}}_{\mathrm{L}} = \boldsymbol{P}_{\mathrm{L}}\,\tilde{\boldsymbol{M}}, \\ \tilde{\boldsymbol{m}}_{\mathrm{R}} = \boldsymbol{P}_{\mathrm{R}}\,\tilde{\boldsymbol{M}}. \end{cases} \tag{1}$$

3. Result and Discussion

Figure 2 shows successive images of pellet ablation with monocular vision. The sampling time and exposure time are 33.75 μs and 10 μs, respectively. The light emission from a pellet plasmoid is typically three-orders of magnitude more intense than the background plasma. In order to express the relatively feeble light emission, the 12 bit dynamic range of the light intensity is expressed using multiple colors which emphasizes the feeble light as shown by the color bar. The cigar-shaped light emission in each frame is high-density and weakly-ionized pellet ablated material, namely, a pellet plasmoid. The major axis of the cigar-shaped light emission is extends along the magnetic field line. The point to observe is that there are one or more weakly emitted distinct region of light emission besides the pellet plasmoid in each frame. This observation can be explained satisfactorily when a breakaway of the pellet plasmoid in the direction perpendicular to the magnetic field line is assumed, namely, some part of the pellet ablated materials are transported from the ablating place across the magnetic field line. Since multiple sep-

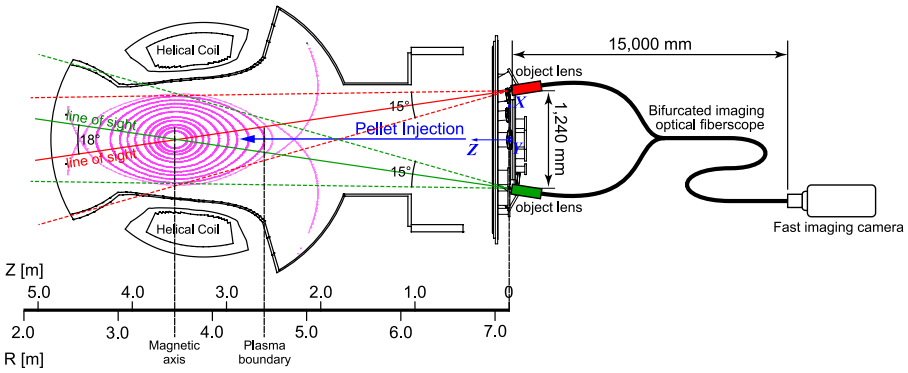

Fig. 1 Horizontal cross section of the LHD. Pellet is injected from the outboard side midplane. Two object lenses of the bifurcated imaging optical fiberscope are mounted viewing in the direction of pellet trajectory with a 1.24 m separation. Each object lens has a 15 degree field of view angle and can observe the whole plasma cross section.

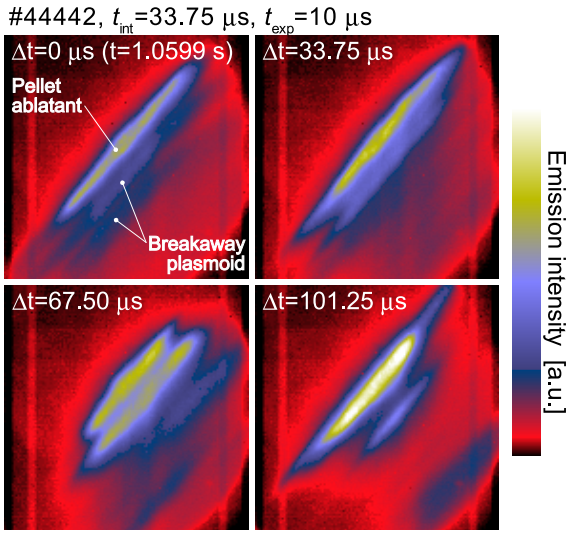

Fig. 2 Typical fast camera images of pellet ablation with monocular vision. Sampling and exposure time of the images are t_{int} = 33.75 μs and t_{exp} = 10 μs. This image is taken obliquely from behind of pellet trajectory. Several cigar-shaped plasmoids which expand along field lines appear in a frame.

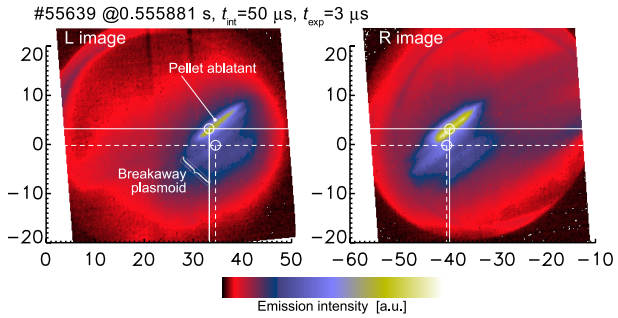

Fig. 3 Typical stereo pair of images of pellet ablation. The epipolar lines of these images are horizontally aligned with each other. Sampling and exposure time of the images are t_{int} = 50 μs and t_{exp} = 3 μs, respectively.

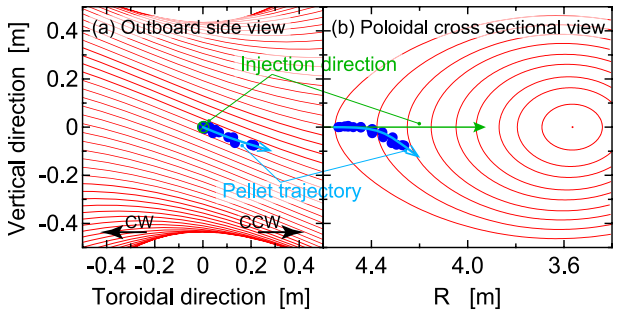

Fig. 4 Projection of the path of the pellet ablated position on (a) the outboard side view, and (b) the poloidal cross-sectional view. Green arrows indicate the initial pellet injection direction. Blue filled circles indicate the measured pellet ablated position, which is defined as the most luminous point in the pellet plasmoid.

arated plasmoid appear within a frame with 10 μs exposure time, it is considered that the minimum interval of the plasmoid separation is more than 100 kHz. At the same time, there is no breakaway plasmoid which can be observed through the several frames, therefore the lifetime of the breakaway plasmoid is shorter than the sampling time (33.75 μs) of the fast camera. These facts suggest that there is a rapid cross-field mass transport from the pellet ablation position within a sufficiently short period of time compared with the pellet lifetime (∼ 1 ms) and the effective pellet deposition profile must be modified from the initial pellet ablation distribution. Therefore, it is very important to clarify the rapid transport mechanism of the pellet plasmoid in addition to the pellet ablation. The direction of motion and the amount of the transported plasmoid are especially essential data from the standpoint of fueling efficiency. In order to investigate the plasmoid behavior, stereoscopic fast imaging camera observation has been employed.

A typical stereo pair of the pellet plasmoid, which is observed in an NBI heated plasma, is shown in Fig. 3. The sampling rate and exposure time are 50 μs and 3 μs, respectively. Here, the most luminous point is chosen as a representative of the pellet plasmoid. When the most luminous point is chosen in the left image ($\boldsymbol{m}_L$), the epipolar line which is corresponding to the left image point is determined by epipolar constraint [14] in the right image. The most luminous point on the epipolar line is the corresponding point in the the right image ($\boldsymbol{m}_R$). The three-dimensional spatial coordinates of the most luminous point ($\boldsymbol{M}$) can be determined from the pair of the corresponding two-dimensional image coordinates $\boldsymbol{m}_L$ and $\boldsymbol{m}_R$ by solving Eq. (1). It is reasonable to assume that a pellet substance is at the most luminous point that indicates the highest density region of a plasmoid, because the pellet is a particle source of the plasmoid. Figure 4 shows the plot representing three-dimensionally measured most luminous points in each frame, i.e., the path of the pellet ablation position. The projected paths on the outboard side view and the poloidal cross-sectional view are shown in (a) and (b), respectively. Green arrows indicate the direction of pellet injection from an outboard side midplane in a horizontally elongated poloidal cross section. Red lines in (a) and (b) indicate the field lines at the pellet ablation position (ρ = 0.89) and the magnetic surfaces structure at the pellet injection cross section, respectively. The pellet trajectory deviates from the initial pellet injection direction while penetrating into the plasma. The trajectory deviation in the direction orthogonal to the pellet injection axis matches the pitch angle of the field line in the counter-clockwise (CCW) direction. This phenomenon is explained by the unbalanced high-energy passing particle distribution that originate from tangential neutral beam injection (NBI) heating. This leads to asymmetric solid

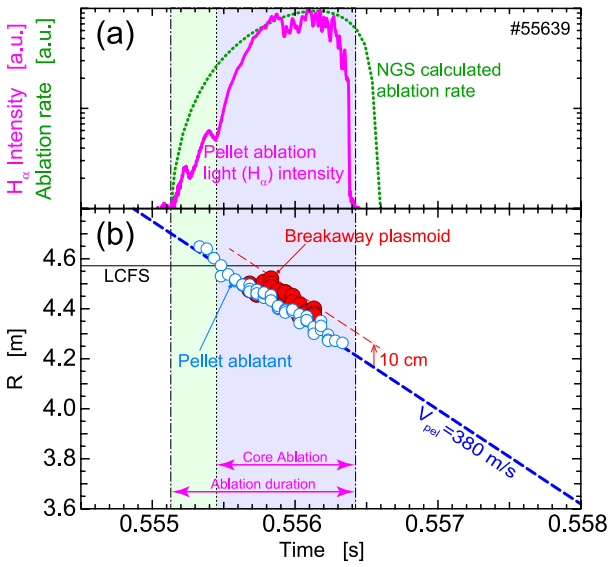

Fig. 5 Time change of, (a) measured pellet ablation light emission intensity with H_α filter (solid-line) and predicted ablation rate with NGS model calculation (dotted-line) on a logarithmic scale, and (b) the pellet ablatant (open-circles) and breakaway plasmoid (filled-circles) position which are reconstructed by stereo observation. Broken-line indicates predicted pellet position when constant velocity is assumed during ablation.

hydrogen ablation on the pellet surface, and the pellet is thrusted by an unbalanced jet of the ablatant [15]. Because a CCW tangentially injected neutral beam is employed in this experiment, high-energy passing particles in the CCW direction, which flow into the pellet along the field line, increase the pellet ablation rate on the exposure side. It follows that the pellet is accelerated to the CCW direction by a counteraction of the ablatant jet in the CW direction. The pellet trajectory deviation suggests that the effect of ablation due to high-energy particles cannot be disregarded in order to evaluate the pellet penetration depth in the neutral beam heated LHD plasmas.

Although the pellet trajectory is deviated by the asymmetric ablation, the radial position of the plasmoid is particularly important to evaluate pellet fueling efficiency. Therefore, we focus on the radial position of the plasmoid. Figure 5 (b) indicates the time change of the pellet position in the major radial direction. The thick broken line indicates the predicted pellet position, which is estimated by the initial pellet velocity measured by the passing time at a light-gate assuming a constant velocity during the ablation. The pellet trajectory passes through the outboard last closed flux surface; LCFS at $R = 4.55$ m, and reaches the magnetic axis at $R = 3.6$ m. The stereoscopically measured pellet ablation position, which is projected to the major radius coordinates, over the passage of time during a pellet lifetime is plotted as an open circle. The ablation light emission starts to be observed about 15 cm before the pellet enters inside the LCFS because of pre-ablation in the stochastic layer which encompasses the core plasma. Correspondence of the measured pellet position (open circle) with the predicted pellet position (thick broken line) suggests that the initial pellet injection velocity component remains constant during the pellet ablation in spite of the pellet trajectory deviation. Eventually, the pellet penetrates to $R = 4.25$ m at $t = 0.5564$ s and disappears. Solid and dotted lines in Fig. 5 (a) indicate the time change of the spatially integrated ablation light emission with a narrow-bandpass filter of the Balmer series α line (656.3 nm) and the calculated pellet ablation rate by the ABLATE code [16] which is based on the NGS model [17] in which only mono energetic electron heating is considered, respectively. The measured lifetime of the pellet is about 15% shorter than that of the NGS model prediction. A possible explanation of the discrepancy between the measurement and predicted pellet lifetime is that the fast ion energy flux due to high energy neutral beam injection enhances the ablation rate in the case of the LHD as mentioned previously [18]. Let us now attempt to extend the stereoscopic observation to the breakaway plasmoid. The breakaway plasmoid is observed as the weakly emitted striation beside the pellet plasmoid as previously mentioned. In the stereo pair images shown in Fig. 3, the position of the breakaway plasmoid (dotted line) relative to the pellet ablation position (solid line) in the left image is shifted to the right and that in the right image is shifted to the left. From such a parallax between the stereo pair images, it can be intuitively understood that the breakaway plasmoid is situated in the foreground of the pellet ablation position. The absolute positions of the breakaway plasmoid in the major radius direction have been reconstructed by the stereo method and plotted as filled circles in Fig. 5 (b). The breakaway plasmoid deviates from the predicted pellet position and always observed in the direction opposite the pellet movement toward the center of the plasma. The maximum distance to breakaway plasmoid from the pellet plasmoid position in which the pellet is ablating is 0.1 m. Since a lifetime of the breakaway plasmoid is shorter than a frame time of the fast imaging camera, a motion of the breakaway plasmoid is not clear. But it can be asserted with confidence that the part of the pellet ablated materials being rapidly transported outward across the field line within a frame time, 50 μs. The effective pellet deposition profiles which are estimated from the difference of the electron density profiles in the Thomson scattering measurement before and 4 ms after pellet ablation, the measured pellet ablation light emission with an H_α filter and the calculated ablation rate profiles are plotted in Fig. 6. The ablation light emission peak is at around $R = 4.3$ m, and this peak position is approximately consistent with the calculated ablation peak position. If the pellet particle is deposited in the flux surface where the pellet is ablated, the particle deposition profile should coincide with pellet ablation profile. However, the peak of

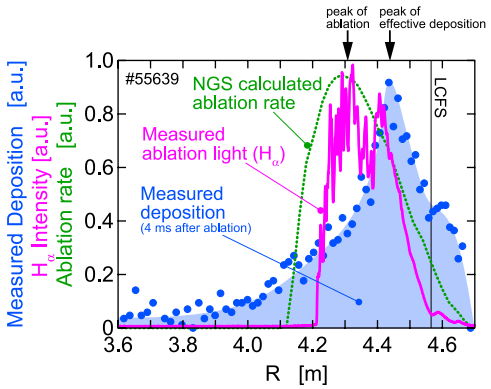

Fig. 6 Profile of measured pellet ablation light emission intensity which is mapped to major radius by assuming constant pellet velocity (solid line), NGS model calculated ablation rate (dotted-line) and measure deposition profile which is estimated from the difference of electron density profiles before and 4 ms after pellet ablation (filled-circles).

the effective particle deposition profile is shifted outward and located around $R = 4.43$ m. Although the density of the breakaway plasmoid is unknown, the difference between the peak position of the pellet ablation and that of the effective particle deposition location is almost coincident with the distance of motion of the breakaway plasmoid. It is reasonable to suggest that the breakaway plasmoid transports the pellet ablated material non-diffusively in a short period of time. Since the drift of the breakaway plasmoid is local and due to fast particle transport before homogenization, it is impossible to measure the density change during transport. The particle deposition profile which can be estimated by Thomson scattering measurement includes not only the pellet ablation profile but also the overall homogenization process of the pellet plasmoid. The outward motion of the breakaway plasmoid is qualitatively similar to the $\nabla \boldsymbol{B}$ induced drift of the pellet plasmoid in tokamaks. However, it is somewhat doubtful whether the pellet plasmoid drift model on tokamaks is directly applicable to LHD or not because the tokamak's model is premised on an axisymmetric two-dimensional magnetic field structure which varies in proportion to $1/R$ [6] while the LHD has a three-dimensional magnetic field structure due to the helical external coils. Advanced modeling that takes into account the three-dimensionality of the helical magnetic configuration is required in order to identify the $\nabla \boldsymbol{B}$ induced drift effects in the LHD plasmas.

4. Conclusion

Experimental observation of the ablating pellet has been performed by employing a fast imaging camera with stereoscopic vision on the LHD. The breakaway and acceleration of the pellet ablatant are observed during the solid hydrogen pellet ablation process.

The breakaway recurrently develops at rate of about 100 times per millisecond and the velocity of the breakaway plasmoid is estimated to far exceed the pellet injection velocity in the direction opposite to the pellet injection. These observations suggest that there is a non-diffusive rapid transport of the pellet ablatant simultaneously with the pellet ablation and therefore, a part of the ablated pellet mass is promptly lost from a flux surface in which the pellet is ablated. This fact suggests that it is important to evaluate the non-diffusive rapid transport of the breakaway plasmoid in addition to the pellet ablation to understand the pellet fueling properties with sufficient accuracy. Since the sampling rate of the fast imaging camera is insufficient to track the movement of the breakaway plasmoid, another means for the observation with higher time resolution is required for further investigation of the dynamics of the breakaway plasmoid.

Acceleration of the breakaway plasmoid in the low magnetic field side direction is clarified by employing stereoscopic observation. The plasmoid behavior is qualitatively consistent with the $\nabla \boldsymbol{B}$ induced drift in a tokamak. It is reasonable to suggest that a common mechanism lies behind both systems due to the similarity of the confinement field. However, advanced modeling studies that takes into account three-dimensionality of the helical magnetic configuration are required in order to identify the $\nabla \boldsymbol{B}$ induced drift effects in the LHD plasmas.

Acknowledgement

The authors would like to thank both the LHD experiment and operation groups for their support. We are also grateful to Drs. K. Narihara and I. Yamada for providing with the Thomson scattering data. This work is supported by the Ministry of Education, Sports, Culture, Science and Technology, Grants-in-Aid for Scientific Research (C)19560831 and (C)21560863.

[1] S.L. Milora *et al.*, Nucl. Fusion **35**, 657 (1995).
[2] B. Pégourié *et al.*, Plasma Phys. Control. Fusion **49**, R87 (2007).
[3] L.R. Baylor *et al.*, Nucl. Fusion **37**, 445 (1997).
[4] P.T. Lang *et al.*, Phys. Rev. Lett. **79**, 1487 (1997).
[5] L.R. Baylor *et al.*, Fusion Technol. **34**, 425 (1998).
[6] V.A. Rozhansky *et al.*, Plasma Phys. Control. Fusion **37**, 399 (1995).
[7] P.B. Parks *et al.*, Phys. Plasmas **7**, 1968 (2000).
[8] B. Pégourié *et al.*, Nucl. Fusion **47**, 44 (2007).
[9] L.R. Baylor *et al.*, Nucl. Fusion **47**, 443 (2007).
[10] R.D. Durst *et al.*, Nucl. Fusion **30**, 3 (1990).
[11] J. de Kloe *et al.*, Phys. Rev. Lett. **82**, 2685 (1999).
[12] H.W. Müller *et al.*, Phys. Rev. Lett. **83**, 2199 (1999).
[13] R. Sakamoto *et al.*, Rev. Sci. Instrum. **76**, 103502 (2005).
[14] R. Hartley and A. Zisserman, *Multiple View Geometry in Computer Vision, Second edition* (Cambridge University Press, 2003).
[15] R. Sakamoto *et al.*, Nucl. Fusion **44**, 624 (2004).
[16] Y. Nakamura *et al.*, Nucl. Fusion **26**, 907 (1986).
[17] P.B. Parks and R.J. Turnbull, Phys. Fluids **21**, 1735 (1978).
[18] M. Hoshino *et al.*, Plasma Fusion Res. **1**, 033 (2006).